International Journal of Sediment Research 32 (2017) 155–170

Contents lists available at ScienceDirect

International Journal of Sediment Research

journal homepage: www.elsevier.com/locate/ijsrc

Original Research

Experiments on the effect of inflow and outflow sequences on suspended sediment exchange rates

Michael Müller [a,b,*,1], Giovanni De Cesare [b], Anton J. Schleiss [b]

[a] IUB Engineering Ltd, Berne, Switzerland
[b] Laboratory of Hydraulic Constructions (LCH), Ecole Polytechnique Fédérale de Lausanne (EPFL), Station 18, CH-1015 Lausanne, Switzerland

ARTICLE INFO

Article history:
Received 21 September 2015
Received in revised form
24 January 2017
Accepted 7 February 2017
Available online 20 February 2017

Keywords:
Laboratory experiments
Inflow and outflow sequences
Suspended sediment
Sediment exchange rates
Turbidity measurements

ABSTRACT

In laboratory experiments, the influence of inflow and outflow sequences on the behavior of fine sediment was investigated. The experimental set-up consisted of two interconnected rectangular basins, between which water was moved back and forth. Suspended sediment concentration in the main basin as well as the sediment exchange rates were derived from turbidity measurements.The suspended sediment ratio, *SSR*, and sediment exchange rates (influx sediment rate, *ISR*, and evacuated sediment rate, *ESR*) were measured. In twenty test runs, a parametric study on the magnitude and frequency of inflow and outflow cycles, the relative duration between inflow and outflow sequences, the initial sediment concentration, and the intake position was done. An initial test with stagnant water described the settling behavior of fine sediment and served as a reference scenario.The test results show that settling of fine particles near the intake/outlet structure can be considerably reduced by the nature of the inflow and outflow sequences. High cycle magnitude and frequency lead to maximum suspended sediment ratio in the system. For low discharges, the evolution of suspended sediment concentration cannot be directly correlated to the inflow and outflow cycles. However, compared to "no operation" conditions, the suspended sediment ratio could be increased by 10% to 40% locally. For high discharge, the evolution of suspended sediment concentration correlated with discharge cycles and suspended sediment ratios between 50% and 80% higher than for stagnant water could be achieved. Similar ratios could be obtained when the intake is located closer to the bottom or to the free water surface.Meanwhile, the overall sediment balance remained in equilibrium over the test period, indicating that the influx and evacuated sediment rates are not significantly influenced by the inflow and outflow cycles.

1. Introduction

Reservoir sedimentation affects many of the storage facilities for drinking water supply, flood retention, and/or hydropower production (Batuca & Jordaan, 2000). When dam construction interrupts the continuity of sediment transport in a river, the deposition and settling processes of the particles supplied from the upstream catchment area start filling up the reservoir. In the case of hydropower, the accumulating sediment reduces the storage capacity as well as operational efficiency and consequently endangers both sustainability and safety of the plants (Basson, 2009; Knoblauch et al., 2005; Müller, 2012; Müller et al., 2014; Schleiss et al., 2010). Deposits in front of intake/outlet structures or clogging of bottom outlets can lead to flow perturbations and safety concerns (Boillat & Delley, 1992; Boillat & Pougatsch, 2000).

In Alpine storage reservoirs the main sedimentation process is turbidity currents, taking place generally during annual flood events, mainly during peak inflow (De Cesare et al., 2001; Schleiss et al., 2016). According to the density difference, the sediment-laden flow follows the thalweg to the deepest area of the reservoir, which is normally close to the dam and/or the power intakes, forming a so-called muddy lake. For storage hydropower plants, several measures against turbidity current driven sedimentation have been studied (Oehy et al., 2010; Oehy & Schleiss, 2007), i.e. obstacles stopping the current propagation or maintaining particles in suspension in front of intakes to be evacuated by the turbines. A similar approach has been investigated by Jenzer Althaus (2011), who studied the effect of a rotating jet induced flow close

* Corresponding author at: Laboratory of Hydraulic Constructions (LCH), Ecole Polytechnique Fédérale de Lausanne (EPFL), Station 18, CH-1015 Lausanne, Switzerland.
E-mail addresses: michael.mueller@iub-ag.ch (M. Müller), giovanni.decesare@epfl.ch (G. De Cesare), anton.schleiss@epfl.ch (A.J. Schleiss).
[1] Formerly at Laboratory of Hydraulic Constructions (LCH), Ecole Polytechnique Fédérale de Lausanne (EPFL), Station 18, CH-1015 Lausanne, Switzerland

http://dx.doi.org/10.1016/j.ijsrc.2017.02.001
1001-6279/

Nomenclature

Symbols

B	Width [m]
C	Suspended sediment concentration [g/l]
C_{calc}	Concentration estimated using the calibration equation [g/l]
D	Diameter [m]
d_m	Mean particle diameter [μm]
d_s	Diameter of the particle [m]
ERR_C	Average error of concentration estimates [g/l]
ESR	Evacuated sediment rate [-]
f	Frequency [Hz]
H	Height [m]
INC_{SSR}	Normalized increase of suspended sediment ratio [-]
ISR	Influx sediment rate [-]
Kt_P	Frequency of inflow and outflow cycles [-]
L	Length [m]
M	Sediment mass [g], [kg], [t]
M_{susp}	Suspended sediment mass [g]
n	Number of sampling points or samples [-]
Q	Discharge [m^3/s], [l/s]
SB	Sediment balance [-]
SSR	Suspended sediment ratio [-]
SSR_{Ref}	Suspended sediment ratio in stagnant water [-]
t	Time [s]
t_m	Mean residence time [s]
t_P	Time to peak for inflow or outflow sequence [s]
TU	Turbidity [FNU]
V	Volume [m^3]
z_i	Position of the intake/outlet structure above the reservoir bottom [m]
ΔH	Height variation [m]
λ	Scale factor [-]
λ_L	Geometric scale factor [-]
$\lambda_{v,t,Q}$	Kinematic scale factor [-]
ν	Kinematic viscosity [m^2/s]
ρ	Density [kg/m^3]

Indices

0	Initial
final	End of the experiment
IN	Inflow
i	Intake
MB	Main basin
MT	Mixing tank
m	Mean
max	Maximum
mod	Model
OUT	Outflow
P	Peak
prot	Prototype
Ref	Reference
S	Sediment or solid
turb	Turbulent
w	Water

to intake structures on sediment mixing in order to evacuate fine sediment through the power intakes.

Further experimental research on suspended sediment behavior in reservoirs was done by Yu et al. (2000), describing the deposition behavior in the muddy lake area, by Qi et al. (2000), analyzing sediment re-suspension by a turbulent jet in an intake pond, by Kantoush et al. (2008), focusing on shallow flows as well as by Toniolo and Schultz (2005), studying trap efficiency of a reservoir depending on the outlet location.

Sediment can be kept in suspension by jet induced flow. In industrial applications, jet mixing has become an alternative to conventional impeller mixing (Wasewar, 2006). Numerous experimental studies on sedimentation and deposition from particle laden turbulent jets and plumes have been carried out (Cardoso & Zarrebini, 2001a, 2001b; Cuthbertson & Davies, 2008; Ernst et al., 1996; Lane-Serff & Moran, 2005). However, the effect of repetitive inflow and outflow sequences and the influence of their amplitude and frequency on fine sediment behavior have not been investigated so far.

Pumped-storage activity alters reservoir stratification and particle dynamics (Anderson, 2010; Bonalumi et al., 2011; Imboden, 1980; U.S. Bureau of Reclamation, 1993). Inspired by the operating mode of pumped-storage plants, a new approach of keeping fine particles in suspension was investigated by Müller(2012) with the idea that fine sediment deposition in the area of intake/outlet structures could be reduced due to the turbulence induced by an adequate plant operation. As a part of that research, prototype turbidity monitoring in the pressurized system of an Alpine pumped-storage plant revealed correlation between short term evolution of suspended sediment concentration and pumped-storage sequences (Müller et al., 2014).

The experimental approach of the doctoral thesis (Müller, 2012) is presented in this paper. The objective is to experimentally investigate how repetitive inflow and outflow sequences affect the settling processes of suspended sediment and the sediment balance of the system. Specifically, the influence of magnitude and frequency of inflow and outflow cycles, relative sequence duration, initial sediment concentration, and intake position on suspended sediment ratios and sediment exchange rates is addressed. The paper describes the experimental set-up and the measuring equipment. Parameter variations, measurement uncertainties, and the different test configurations are presented and results are discussed.

2. Test facility and instrumentation

The laboratory experimental facility consisted of two basins interconnected by a reversible water circuit for generating inflow and outflow sequences. Discharge was regulated and controlled during the experiment, flow velocities were recorded using Ultrasonic Velocity Profilers (UVP) and turbidity in both basins was continuously measured. The set-up and the measuring techniques are described in the following sections.

2.1. Main basin with intake/outlet

Most of the relevant measurements were carried out in the rectangular main basin (subscript *MB*, Fig. 1). It has an inner length of L_{MB}=4.0 m, an inner width of B_{MB} = 2.0 m and a height of H_{MB}=1.5 m. One lateral wall and the front wall are made of glass for flow visualization, where as the other walls and the horizontal bottom are made of steel.A perforated steel plate is inserted vertically at 0.5 m from the back wall to disconnect the test chamber from the zone influenced by the feeding conduit, the security

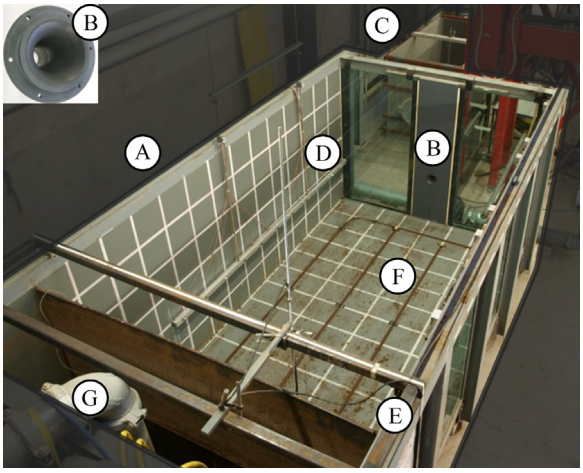

Fig. 1. Photo of the laboratory set-up; A is the main basin; B, the intake/outlet; C, the mixing tank; D, the frame with UVP sensors; E, the movable frame with the turbidity probe; F, the pressurized air supply; and G, the feeding conduit for initial filling of the system.

spillways, the purge outlet, and the pressurized air supply of the main basin.

The water intake/outlet is located at the front wall and can be placed at z_i=0.25, 0.50, or 0.75 m above the reservoir bottom. The water intake has been designed to reduce head losses and turbulence disturbing the flow in the vicinity of the structure (Jenzer Althaus, 2011). It consists of an elliptical bell mouth shaped intake followed by a cylindrical throat with an inner diameter of D_i=48 mm (detail B in Fig. 1).

2.2. Mixing tank

The mixing tank (subscript *MT*, C in Fig. 1) consists of a rectangular prismatic tank with vertical PVC walls reinforced by steel frames. With its inner dimensions of L_{MT}=1.98 m, B_{MT}=0.98 m, and H_{MT}=1.06 m, it provides a volume of approximately V_{MT}=2 m^3. Similar to the main basin it is equipped with a pressurized air supply for mixing purposes at the beginning of the experiments.This basin provides mixing possibility and storage volume to move water from or to the main basin. Thus, the mixing tank intake/outlet is not specially designed and just consists of a conduit entering the tank at z=0.25 m above the bottom.

2.3. Flow diverter

A flow diverting system of soft plastic and rigid aluminum pipes (Fig. 2) allowed flow operation in the two directions defined as follows:

1. *IN*-sequence water entering the main basin (inflowing jet)
2. *OUT*-sequence water withdrawn from the main basin (outflow)

A rigid conduit of diameter D=4.8 cm and length L=1.5 m between the flow diverting system and the intake/outlet of the main basin assures uniform approach flow (straight jet) especially during the inflow sequences. Discharge is measured by an electromagnetic flow meter and regulated by a pump. The semi-rigid diverting conduits are connected by four small manual valves which allow the flow direction to be changed during the experiment.

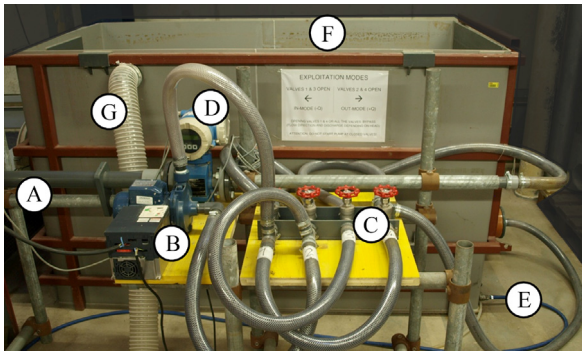

Fig. 2. Mixing tank and flow diverting system; A is the rigid PVC conduit to the main basin; B, the pump and its velocity regulator; C, the flow diverting valves; D, the flow meter; E, the pressurized air supply; F, the mixing tank; and G, the security spillway connected to a sewer.

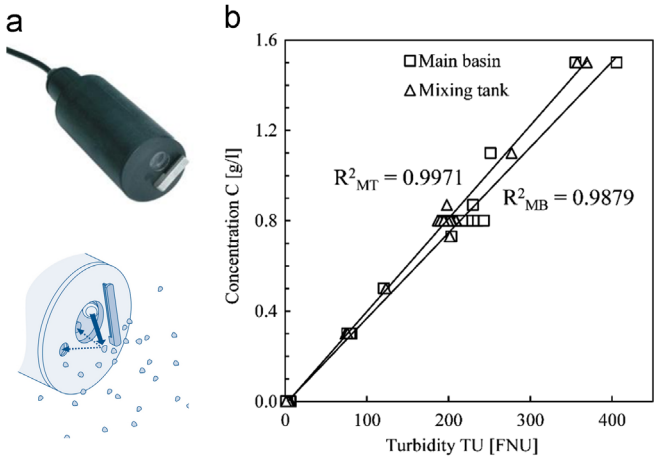

Fig. 3. Photo (above) and measuring system (below, source: HACH LANGE manual) of the *SOLITAX sc* turbidity sensor (a) and turbidity calibration curve for the two probes (b).

2.4. Turbidity probe

The turbidity in the two basins was measured by two *SOLITAX sc* sensors (HACH LANGE, Germany, Fig. 3a) connected to the acquisition and display system *SC100 Controller* of the same manufacturer. Based on an infrared absorption scattered light technique, the probe determines the turbidity in the sampled water. In the present study, turbidity values were acquired at a frequency of f=0.2 Hz. The linear relation between the turbidity *TU* [FNU] and the suspended sediment concentration *C* [g/l] was determined in the laboratory for known sediment concentrations from C=0.3 to 1.5 g/l. In addition, the initial sediment concentrations, C_0, at the beginning of each test run were considered as validation points. The following calibration relation was derived (Fig. 3b):

$$C_{MB} = 0.0038 \cdot TU_{MB} - 0.0099 \quad (1)$$

$$C_{MT} = 0.0041 \cdot TU_{MT} - 0.0138 \quad (2)$$

where C_{MB}: the suspended sediment concentration in the main basin [g/l], C_{MT}: the suspended sediment concentration in the mixing tank [g/l], TU_{MB}: the measured turbidity in the main basin [FNU], and TU_{MT}: the measured turbidity in the mixing tank[FNU].

In the main basin, the turbidity sensor was installed in the opposite quadrant to the UVP measurements. During the experiments, the concentration was continuously recorded at the intake height, z_i. After every third flow reversal, the probe was temporally

moved vertically to evaluate the vertical distribution of suspended sediment. In the mixing tank, the measuring point is located in the center of the chamber at the height of the inflow/outflow conduit.

It is assumed that the point measurement of suspended sediment concentration is representative for the whole test chamber, thus, an uncertainty due to possible spatial variations of the suspended sediment concentration is accepted. The root mean square error of the concentration measurements was determined using the sampled *TU-C* pairs. The average error, ERR_C, is:

$$ERR_C = \sqrt{\sum \frac{(C_{calc} - C_0)^2}{n-1}} \quad (3)$$

where C_{calc}: the concentration [g/l] estimated using the calibration equation, C_0: the known initial concentration [g/l] applying $C = M/V$, and$n$: the number of samples considered for error estimation [-].The average error introduced due to calibration is $ERR_{C,MB} = \pm 0.048$ g/l for the probe in the main basin and $ERR_{C,MT} = \pm 0.024$ g/l in the mixing tank.

2.5. Ultrasonic velocity profilers

Flow patterns in the main basin were measured with *Ultrasonic Velocity Profilers* (UVP, Met-Flow, Switzerland (Met-Flow SA, 2000)). This technique, developed by Takeda (1995), allows instantaneous velocity profile measurement by using the Doppler shift of echoes reflected by small particles in the fluid. In former studies, turbidity currents and 2D flows in shallow reservoirs were successfully monitored by this flow mapping technique (De Cesare & Schleiss, 1999; Kantoush et al., 2008). Suspended sediment provides an excellent flow tracer and assures high reliability of velocity measurements.

Seventeen 2 MHz UVP transducers were aligned on a movable aluminum frame along the side wall of the test chamber to measure horizontal 2D velocity fields at several levels in the main basin. The configuration with operating UVP azimuth angles of 90° and 45° minimizes the influences of the measuring equipment on the flow conditions. Flow velocity was sampled at 28 points in one quadrant of the test chamber, resulting in 2D flow patterns of 1.0 x 2.0 m^2.

The UVP flow mapping served to observe the temporal development of kinetic energy in the main basin as well as to calibrate a 3D numerical model of the test facility. As this paper is focusing on the behavior of the suspended sediment phenomenon, the results of UVP velocity measurements are not discussed further here.

3. Experimental parameters

3.1. Similarity rule and normalizing parameters

The experiments are carried out respecting the criterion of Froude similarity. The same relationships for inertia and gravity forces apply in prototype (subscript prot) and model (subscript mod). Geometric (L) and kinematic (ν, t, Q) parameters follow the relations

$$\lambda_L = \frac{L_{prot}}{L_{mod}}; \quad \lambda_{\nu,t} = \lambda_L^{1/2}; \quad \lambda_Q = \lambda_L^{5/2} \quad (4)$$

The Reynolds number at the intake/outlet is $7560 \leq Re_i \leq 29,180$ and, thus, turbulent conditions were present for every tested discharge.

The main basin width, B_{MB}, was chosen for normalizing lengths. Velocities and time are normalized by the approach flow velocity in the pipe, $v_0 = Q_{IN,OUT}/A$, and the mean residence time, $t_m = V_{MB}/Q_{IN,OUT}$, respectively. The latter was proposed by Stefan and Gu (1992) to be used for normalization of time in jet mixing problems. However, in the presentation of results there may be some exceptions when real time presentation is necessary for better understanding.

3.2. Sediment material

Settling processes are affected by properties of the surrounding fluid (viscosity, ν, and density, ρ_w) and particle characteristics (diameter, d_S, material density, ρ_S, shape factor, *SF*, and concentration, C_0 (van Rijn, 1984)). The water temperature during the experiments varied between T_w = 14 and 17 °C. Viscosity effects on settling velocity are small in this range and can, thus, be neglected.

The experiments were carried out using walnut shell powder to reproduce the suspended sediment. Previous research showed that this homogeneous material presents ideal behavior to model reservoir sedimentation processes (Jenzer Althaus, 2011; Kantoush et al., 2008). Density is ρ_s =1480 kg/m^3, the mean particle diameter is d_m=121 μm, and the particles are slightly angular shaped. These characteristics allow reproduction of prototype ratios between flow velocities and settling velocities in the reservoir. As organic material is subject to swelling, long-term tests on the behavior of the nutshell powder were carried out. Swelling is negligible over the investigated test duration and does allow correct turbidity measurement.

Tests were carried out for C_0=0.8 g/l in both basins. As sediment concentration influences the settling velocity in a fluid, two experiments were carried out with lower and higher concentrations of C_0=0.3 and 1.5 g/l, respectively, in the two basins.

3.3. Magnitude and frequency of inflow and outflow cycles

The experiments were carried out for five different discharges from Q=0.3 to 1.1 l/s. These magnitudes of the inflow and outflow cycles were given by the volumes of the main basin and the mixing tank and the design of the water intake/outlet (Jenzer Althaus, 2011) as well as by considering discharges, velocities, and residence times of real case pumped-storage plants. The range of chosen cycle magnitudes considering Froude similarity situates the experimental scale at λ_L=50–100 approximately.

The initial frequency of inflow and outflow cycles, Kt_P, was determined through tests by numerical simulations and under clear water conditions. In the numerical model, the temporal evolution of the kinetic energy in the test chamber was evaluated to define the duration needed to achieve steady state conditions during an inflow, outflow, and “no operation” sequence. This energy was calculated as the sum of the flow velocities computed in each grid cell and reached maximum values for a fully developed and constant velocity field. Therefore, the duration to reach steady state conditions in the test chamber was called “time to (reach) peak (energy)”, t_P. This parameter depends on discharge and was determined by pilotphysical modeling and numerical simulation tests. Table 1 lists the mean residence time, t_m, the time to peak, t_P, and corresponding dimensionless time, t_P/t_m, which varies between t_P/t_m=0.099 and 0.136 for the five test discharges.

The base configuration for each discharge consists in five cycles resulting in experiment durations, $10t_P$, between 2 h 15 min and 11

Table 1
Mean residence time, t_m, and time to peak, t_P, for different discharges, Q.

Q [l/s]	t_m [s]	t_P [s]	t_P/t_m [-]
0.3	30,056	4080	0.136
0.5	18,034	2280	0.126
0.7	12,881	1500	0.116
0.9	10,019	1080	0.108
1.1	8197	810	0.099

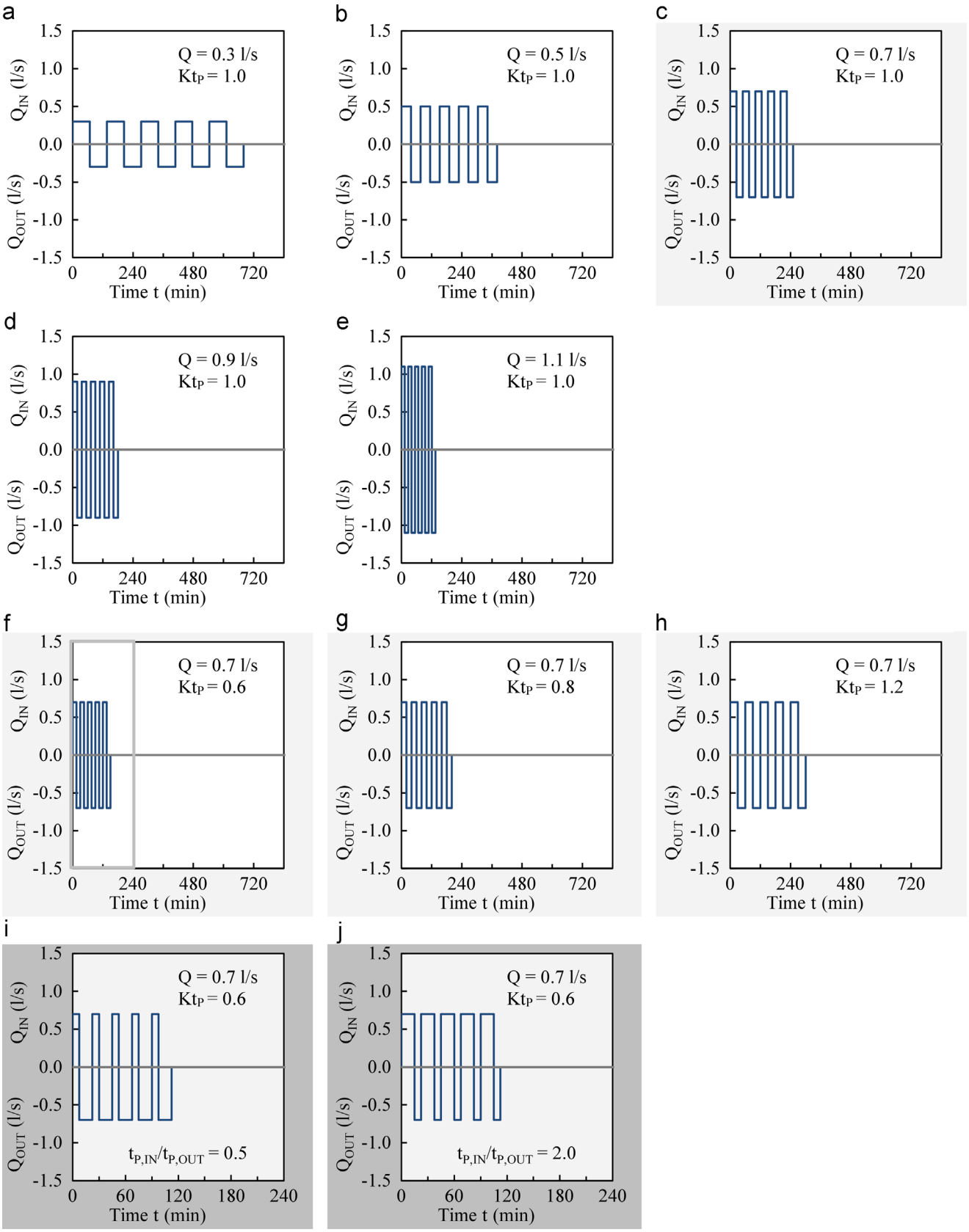

Fig. 4. Selection of ten investigated inflow and outflow cycles. Variation of discharge Q=0.3 (a), 0.5 (b), 0.7 (c), 0.9 (d), and 1.1 l/s (e) for cycle frequency, Kt_P=1.0. Variation of cycle frequency Kt_P=0.6 (f), 0.8 (g), and 1.2 (h) for discharge Q = 0.7 l/s. Variation of relative sequence duration $t_{P,IN}/t_{P,OUT}$=0.5 (i) and 2.0 (j) for discharge Q=0.7 l/s and cycle frequency Kt_P=0.6.

h 20 min (Fig. 4a to e). The shape of the experimental hydrograph is similar to a square wave. Dissipation or "no operation" sequences were not reproduced.Four different cycle frequencies, Kt_P, were studied (Fig. 4f to h). Initial cycle frequency, $Kt_P = 1.0$, means that at the end of each inflow or outflow sequence steady state conditions are achieved in the basin just when flow direction is reversed.Higher frequencies, Kt_P=0.6 and 0.8, implicate faster changes in operation mode and do not allow the development of a constant velocity field in the test chamber before flow reversal. Kt_P=1.2 is assumed to prolongate the steady conditions in the basin before the reversal of flow direction. The variation of cycle frequency was tested for three of the five discharges.

The presented variation of magnitudes and frequencies of inflow and outflow cycles cover quite a wide range of short and long sequences with high and low discharges. However, in engineering applications, such as pumped-storage plants, perfect cyclic behavior of inflow and outflow sequences is rare. In real cases, rather random operational hydrographs with sometimes varying discharges within the proper cycles are observed. Nevertheless, most of the pumped-storage operations present a cyclic behavior, according to daily, weekly, or seasonal production/absorption purpose.

Two additional experiments with a different relative sequence duration, $t_{P,IN}/t_{P,OUT}$, were tested. An inflow sequence occupied double the time of an outflow sequence and vice-versa (Fig. 4i and j).

3.4. Intake/outlet position

Flow patterns in the test chamber are changing when the intake/outlet is located closer to the reservoir bottom or the free surface. With changing flow conditions, the behavior of suspended sediment is expected to be altered as well. Therefore, the position of the intake/outlet structure above the basin bottom, z_i/B_{MB}, was changed for two experiments, from the initial location at z_i/B_{MB}=0.25 to z_i/B_{MB}=0.125 and 0.375 for a discharge of Q=1.1 l/s.

3.5. Experimental procedure

After filling the main basin to $H_{0,MB}$=1.15 m and the mixing tank to its full level $H_{0,MT}$=1.06 m, the two reservoirs are disconnected from the external water supply and are studied as a closed system. For the experiments with sediment, the desired mass of walnut shell powder was mixed with water and poured into the basins. Pressurized air supply on the bottom generated whirling flow conditions to mix and maintain the sediment in suspension. Air bubbles were stopped and inflow and outflow cycles were started at t=0 s. As the total water volume remained constant over the experimental duration, the water level in both basins varied in time. The maximum level variation in the main basin was of $\Delta H_{MB} = \pm 0.18$ m for one cycle.

Suspended sediment concentrations$C$ in the main basin and the mixing tank were continuously measured. UVP measurements were made one to three times per sequence, according to the cycle duration. At the end of a test run, the final sediment content in the mixing tank was measured after resuspending all sediment in the tank.

After having measured the reference settling curve of the sediment under "no operation" conditions, the suspended sediment ratio, SSR, could be defined for each experiment:

$$SSR(t) = \frac{\sum M_{susp}(t)}{M_0} = \frac{M_{susp,MB}(t) + M_{susp,MT}(t)}{M_{0,MB} + M_{0,MT}} \quad (5)$$

where M_{susp}:the suspended sediment mass in the system [g], and M_0: the initial sediment mass in the system [g].

The efficiency of inflow and outflow sequences in keeping the fine sediment in suspension is defined by the normalized increase, INC_{SSR}, of suspended sediment ratio with and without inflow and outflow cycles:

$$INC_{SSR}(t) = \frac{SSR(t) - SSR_{Ref}(t)}{SSR_{Ref}(t)} \quad (6)$$

High values of INC_{SSR} represent high impact of the tested sequences, values close to 0 indicate that the settling behavior of the suspended sediment is only marginally influenced by the inflow and outflow sequences.

4. Experimental results and analysis

4.1. Reference tests

To evaluate the influence of inflow and outflow sequences on suspended sediment ratio, preliminary experiments were done in stagnant water during almost 14 h. Suspended sediment concentration was continuously measured in both tanks at z/B=0.25 above the bottom. Fig. 5 shows the suspended sediment ratio, SSR, as a function of time, t. The settling behavior follows a logarithmic decay.

Periodical samples in the main basin taken at z/B_{MB}=0.125, 0.375, and 0.5 show that the bottom layers of the water body are slightly more turbid (peaks in Fig. 5a). As the settling behavior in

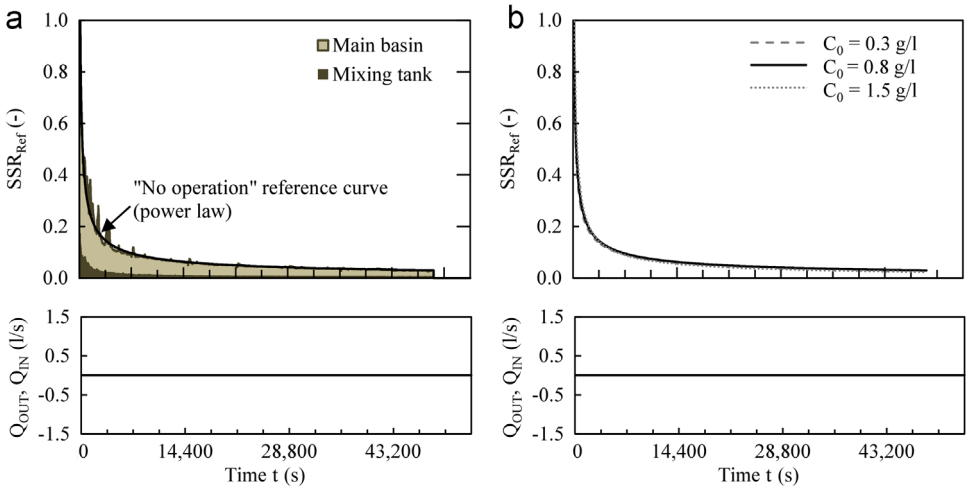

Fig. 5. Suspended sediment ratio, SSR, as a function of time, t, in calm water conditions for initial sediment concentration C_0=0.8 g/l (a) and power law curves for the three different initial concentrations (b).

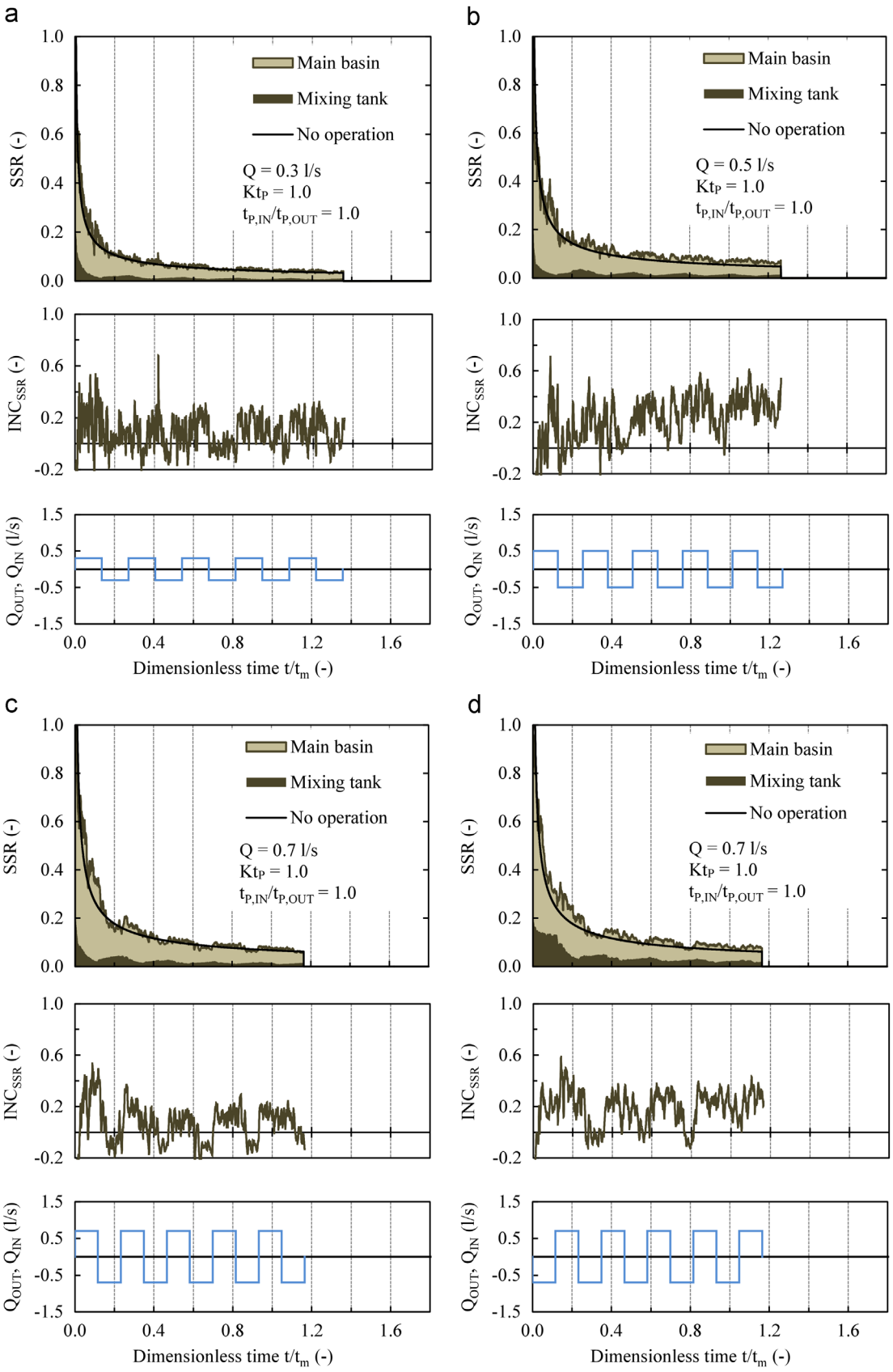

Fig. 6. Suspended sediment ratio, *SSR*, dimensionless increase, INC_{SSR}, and discharge, *Q*, as a function of dimensionless time, t/t_m, for C_0=0.8 g/l, Kt_P=1.0, and Q=0.3 (a), 0.5 (b), and 0.7 l/s (c), and reversed in-out-cycle for C_0=0.8 g/l, Kt_P =1.0, and Q=0.7 l/s (d).

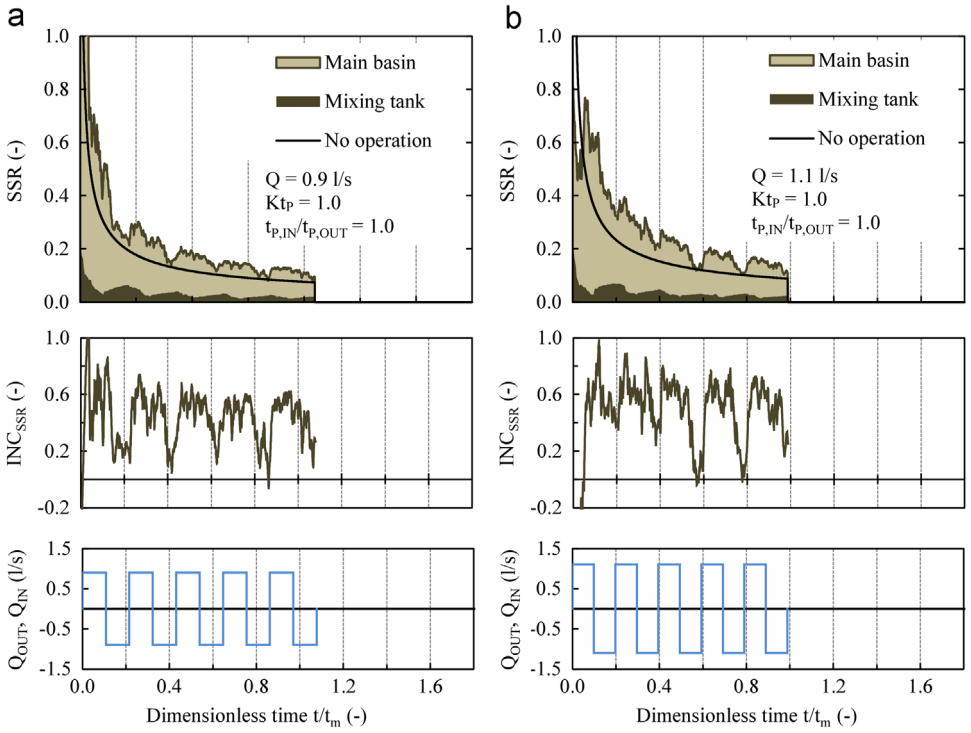

Fig. 7. Suspended sediment ratio, *SSR*, dimensionless increase, INC_{SSR}, and discharge, *Q*, as a function of dimensionless time, t/t_m, for C_0=0.8 g/l, Kt_P=1.0, and *Q*=0.9 (a) and 1.1 l/s (b).

calm water depends on the particle concentration in the test chamber, reference tests were carried out for the two other initial concentrations as well. Fig. 5b reveals that the temporal evolution of *SSR* is very similar for all three cases, hence, no hindered settling occurred under the experimental conditions.

During the first four hours, the suspended sediment ratio drops to a value of approximately *SSR*=0.06. Then, it decreases slowly to about *SSR*=0.03. The base test configuration for *Q*=0.7 l/s and Kt_P=1.0 and with a duration of *t*=15,000 s covers these four hours during which most of the suspended sediment is settling.

The experimental results given hereafter focus on varying cycle magnitude and frequency for C_0 = 0.8 g/l. The influence of initial sediment concentration, C_0, is presented later on.

4.2. Suspended sediment ratio, SSR

Continuous turbidity measurements over the test period determined the suspended sediment concentration at a time step of Δt=5 s during the entire experiment. Knowing the varying volume in the two basins, the suspended sediment mass was calculated and *SSR* defined (Eq. (5)). The relative increase, INC_{SSR}, was calculated.

Figs. 6 and 7 show the *SSR* and INC_{SSR} as a function of dimensionless time, t/t_m, for cycle frequency, Kt_P=1.0, and five different discharges. For discharges *Q*=0.3 and 0.5 l/s, the evolution of the suspended sediment ratio does not clearly correlate with the discharge curve. However, the increased fluctuation of the *SSR* compared to the reference test and the relative increase reveal a final suspended sediment ratio which is approximately 20–30% higher than in stagnant water.

With increasing discharge, the evolution of *SSR* starts to correlate with the discharge cycles. The suspended sediment ratio fluctuates according to inflow and outflow sequences with relative increases between INC_{SSR}=50 and 60% during inflow *Q*=0.9 and 1.1 l/s.

During the first in-out-cycle or until t/t_m=0.2 approximately, the settling process is dominant. Nevertheless, the magnitude of the cycles plays an important role in slowing down this process (Fig. 7). Higher cycle magnitudes lead to increased *SSR* at the end of five inflow and outflow cycles and allow up to 60% more particles in suspension than without inflow and outflow cycles. However, also for *Q*=0.9 and 1.1 l/s, the overall trend of the *SSR* curve is still decreasing by the end of the experiment.Whether the cycles start with an inflow or an outflow sequence only marginally influences the overall *SSR* in the two basins (Fig. 6c and d).

To evaluate if *SSR* can be maintained at a higher level due to the inflow and outflow sequences, the experiments for *Q*=0.9 and 1.1 l/s were prolonged to the absolute duration of the basic configuration (*Q*=0.7 l/s and Kt_P =1.0). Two and five more cycles, respectively, were added to cover the entire main settling phase of approximately four hours defined during reference tests. The comparison is illustrated in Fig. 8 for *Q*=0.3, 0.7, 0.9 and 1.1 l/s. In Fig. 8, *SSR*, INC_{SSR}, and *Q* are plotted as a function of real experimental time to match with results presented for the reference case (Fig. 5). For low discharges, the correlation between suspended sediment ratio and discharge cycles disappears after some 9,000 s of test duration and the fluctuations on the *SSR* curve become smaller. However, *SSR* remains considerably high, with values of INC_{SSR}=50 and 60% for the two highest discharges, i.e. in the same range as after less cycles.

The influence of cycle frequency on suspended sediment ratio is shown in Fig. 9 for *Q* = 1.1 l/s. At increased cycle frequency Kt_P = 0.6 or 0.8, the main basin is assumed not to reach steady state conditions. This is confirmed by the suspended sediment ratio, as it remains high due to the increased cycle frequency, reflecting discharge cycles less clearly than for Kt_P = 1.0 and 1.2. The illustrated behavior of the suspended sediment ratio is also found for the other discharges *Q* = 0.3 and 0.7 l/s.

For Kt_P = 0.8, the relative increase is INC_{SSR} ~80% during inflow sequences, while for Kt_P=0.6, 1.0, and 1.2 it is around 60%. For the other two tested discharges, *Q*=0.3 and 0.7 l/s, a lower relative increase of INC_{SSR}=20–40% is found, according to the results for the cycle magnitude variation.

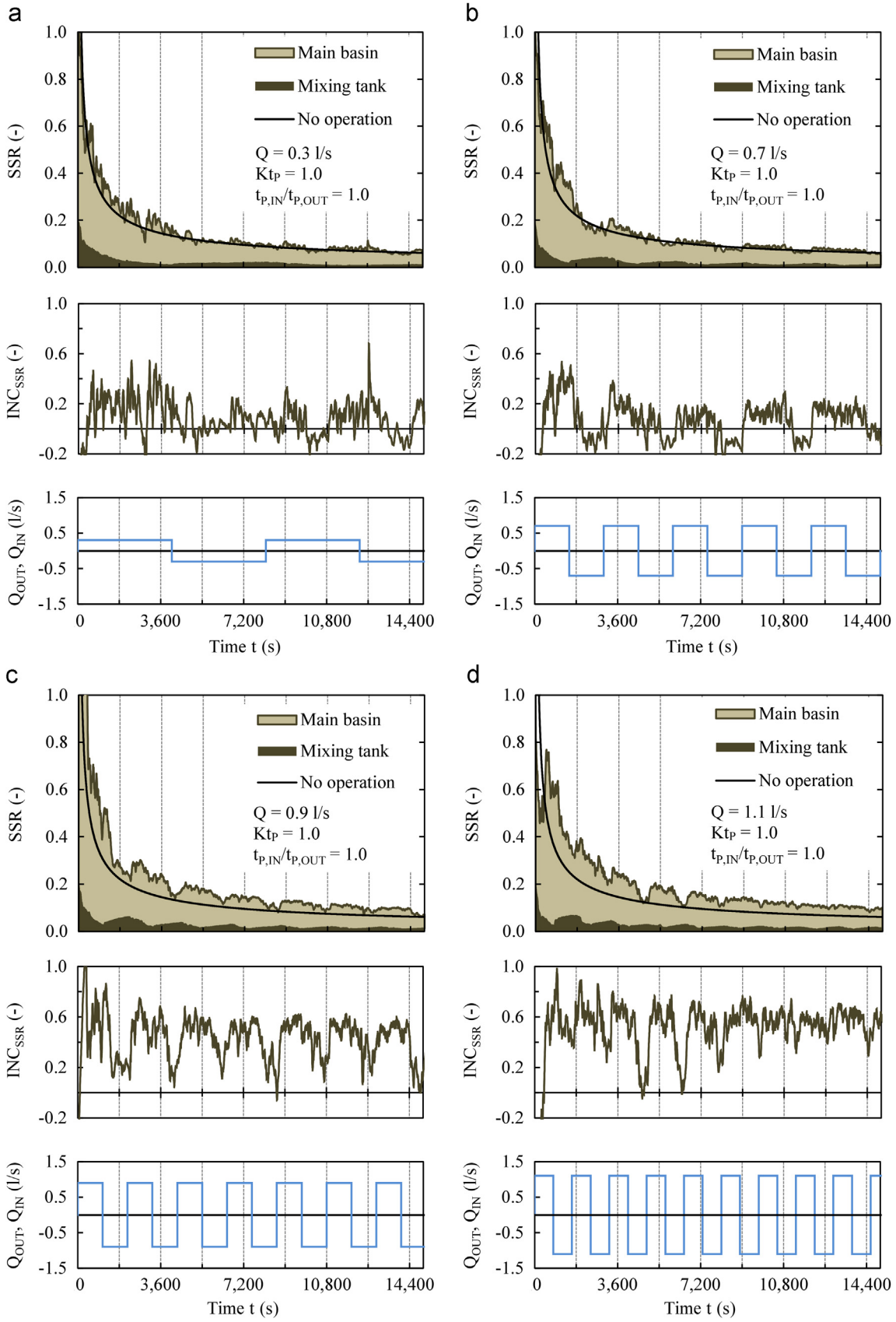

Fig. 8. Suspended sediment ratio, *SSR*, dimensionless increase, INC_{SSR}, and discharge, *Q*, as a function of time, *t*, for $C_0 = 0.8$ g/l, $Kt_P = 1.0$, and $Q = 0.3$ (a), 0.7 (b), 0.9 (c), and 1.1 l/s (d).

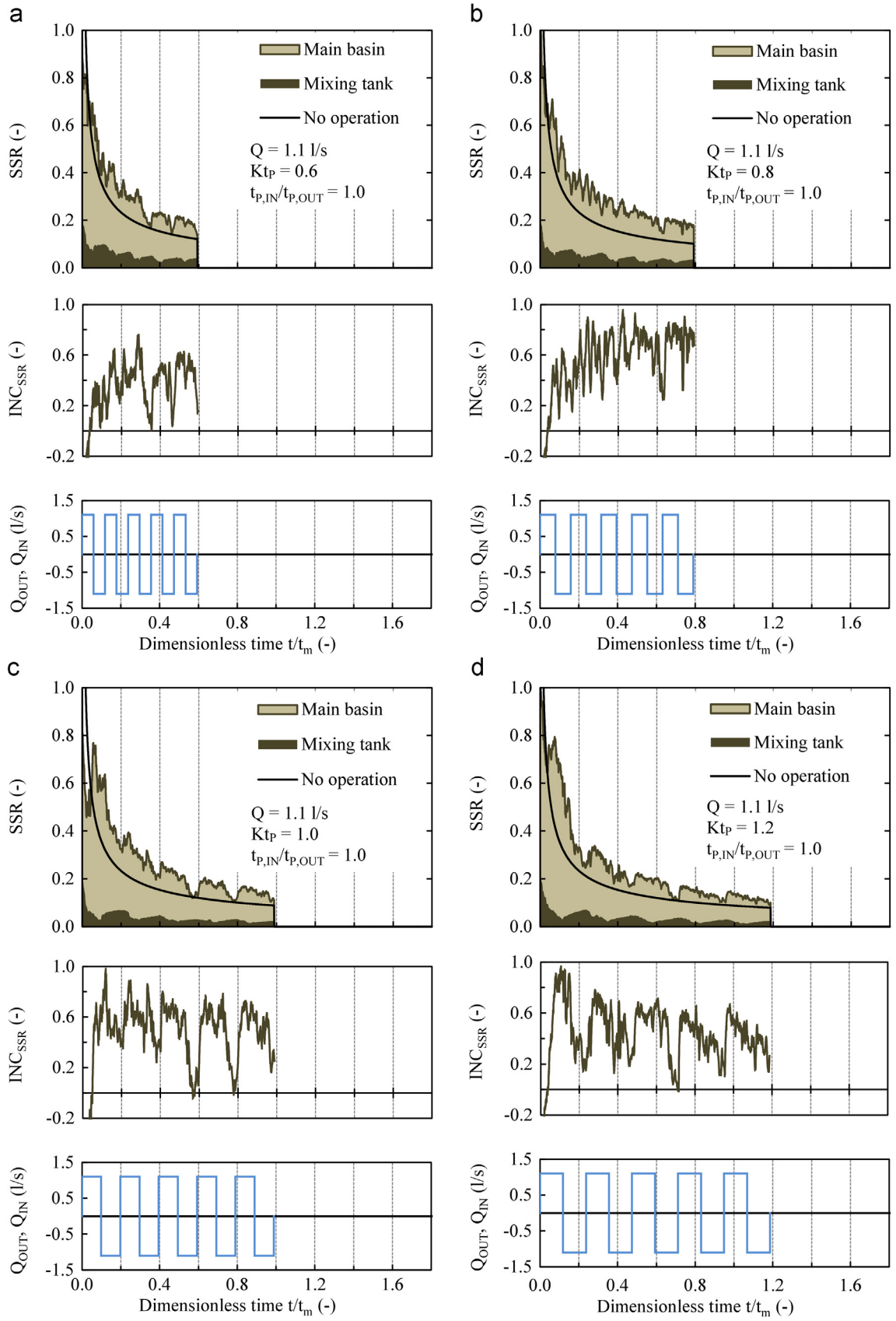

Fig. 9. Suspended sediment ratio, *SSR*, dimensionless increase, INC_{SSR}, and discharge, *Q*, as a function of dimensionless time, t/t_m, for C_0=0.8 g/l, Q=1.1 l/s, and Kt_P=0.6 (a), 0.8 (b), 1.0 (c), and 1.2 (d).

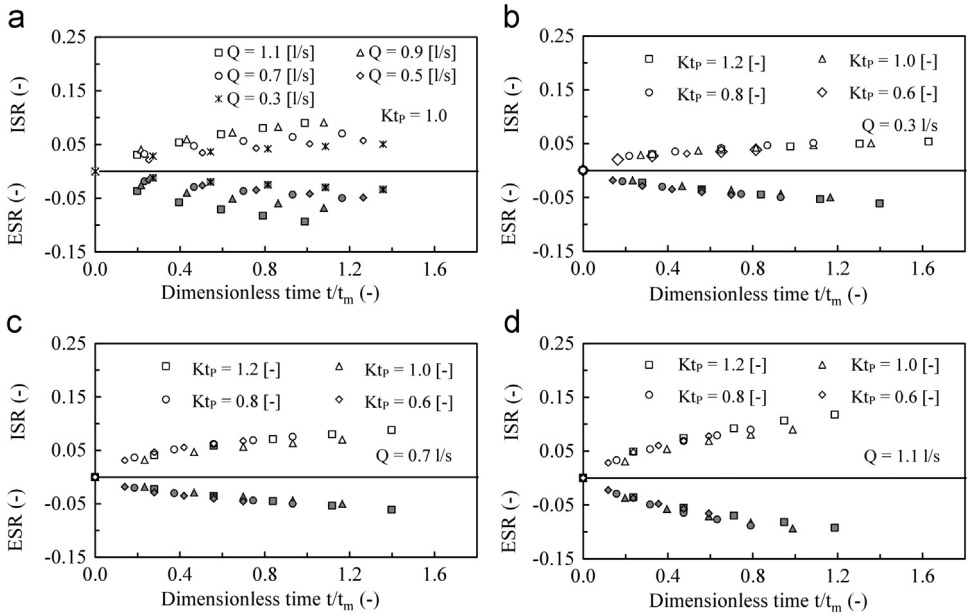

Fig. 10. Influx sediment rate, *ISR*, and evacuated sediment rate, *ESR*, as a function of dimensionless time, t/t_m, for C_0=0.8 g/l, Kt_P=1.0, and different cycle magnitudes Q (a), and for C_0=0.8 g/l with different cycle frequencies, Kt_P, and discharges Q=0.3 (b), 0.7 (c), and 1.1 l/s (d).

4.3. Sediment exchange rates

Assuming a uniform distribution of suspended sediment in the two test chambers, the influx sediment rate, *ISR*, and the evacuated sediment rate, *ESR*, of the main basin can be calculated for each cycle:

$$ISR(t) = \frac{M_{S,IN}(t)}{M_0} = \frac{\sum Q_{IN} \cdot C_{MT}(t) \cdot \Delta t}{M_{0,MB} + M_{0,MT}} \quad (7)$$

$$ESR(t) = \frac{M_{S,OUT}(t)}{M_0} = \frac{\sum Q_{OUT} \cdot C_{MB}(t) \cdot \Delta t}{M_{0,MB} + M_{0,MT}} \quad (8)$$

The evolution of the cumulative influx and evacuated sediment rate are presented in Fig. 10 as a function of t/t_m. The two sediment rates develop practically symmetrically in time, indicating that the sediment balance, *SB*, of the system is almost in equilibrium.

As high cycle magnitude keeps the suspended sediment ratio at a higher level in the system, influx and evacuated sediment rates increase with increasing discharge. The growth rates of the two curves develop proportionally to the suspended sediment ratio, i.e. slope is steeper during the first cycles and then the curves flatten toward the end of the experiment. After five inflow and outflow cycles, *ISR* and *ESR* are both around 9% for Q= 1.1 l/s. For the lowest discharge, Q=0.3 l/s, values around 5% were computed (Fig. 10a).

Cycle frequency affects the final influx and evacuated sediment rate. Longer test duration increases the amount of sediment entering and leaving the main basin. However, Fig. 10b to d reveals that high frequency cycles of Kt_P=0.6 and 0.8 reach, approximately, the same influx and evacuated sediment rates as the lower frequency cycles.

4.4. Sediment balance of the system

The sediment balance, *SB*, of the system was established from the influx (*ISR*) and evacuated sediment rate (*ESR*) for the main basin:

$$SB(t) = \frac{M_{S,IN}(t) - M_{S,OUT}(t)}{M_0} = ISR(t) - ESR(t) \quad (9)$$

The *SB* defines the normalized sediment mass transferred from one reservoir to the other. A negative sediment balance indicates particle evacuation from the main basin.

As previously discussed, the *ISR* and *ESR* developed similarly in time. *SB* calculations confirm this behavior. Even if the transported mass during inflow and outflow sequences is quite high, the sediment balance in the system is not significantly influenced by the inflow and outflow cycles. The sediment balance is -0.03 < *SB* < 0.04 for all tested configurations (Fig. 11). Thus, inflow and outflow cycles move a lot of sediment back and forth but do not contribute to sediment redistribution between the two reservoirs for the chosen experimental set-up.

Neither cycle magnitude nor cycle frequency affect the sediment balance in one or the other direction. However, the relative sequence duration does, as the sediment balance shifts to values between *SB* =-0.03 and 0.03 according to inflowing or outflowing water.

For nearly all test configurations, the sediment balance is positive at the end of the experiment. As the suspended sediment ratio is highest at the very beginning of the experiment, the first inflow sequence leads automatically to the highest sediment input into the main basin over the total test duration. This effect remains unbalanced even if the following inflow and outflow cycles keep transporting sediments from one test chamber to the other. A test with reversed inflow and outflow cycles (Fig. 6d) confirms this statement, presenting a negative sediment balance on the same order of magnitude as the tests starting with an inflow sequence.

5. Discussion

Five parameters were varied for the test series. To discuss the influence of cycle magnitude, Q, and frequency, Kt_P, as well as other parameters relative to sequence duration, $t_{P,IN}/t_{P,OUT}$, initial sediment concentration, C_0, and intake position, z_i, the mean values of suspended sediment ratio, SSR_m, and relative increase, INC_{SSR}, over each inflow and outflow sequence are considered.

For all analyzed cycles, the first inflow and outflow cycle is dominated by the settling process of the sediment. Up to t/t_m=0.2, a decrease to approximately SSR=0.4 is observed. About 60% of the fine sediment settled over this period, almost independently

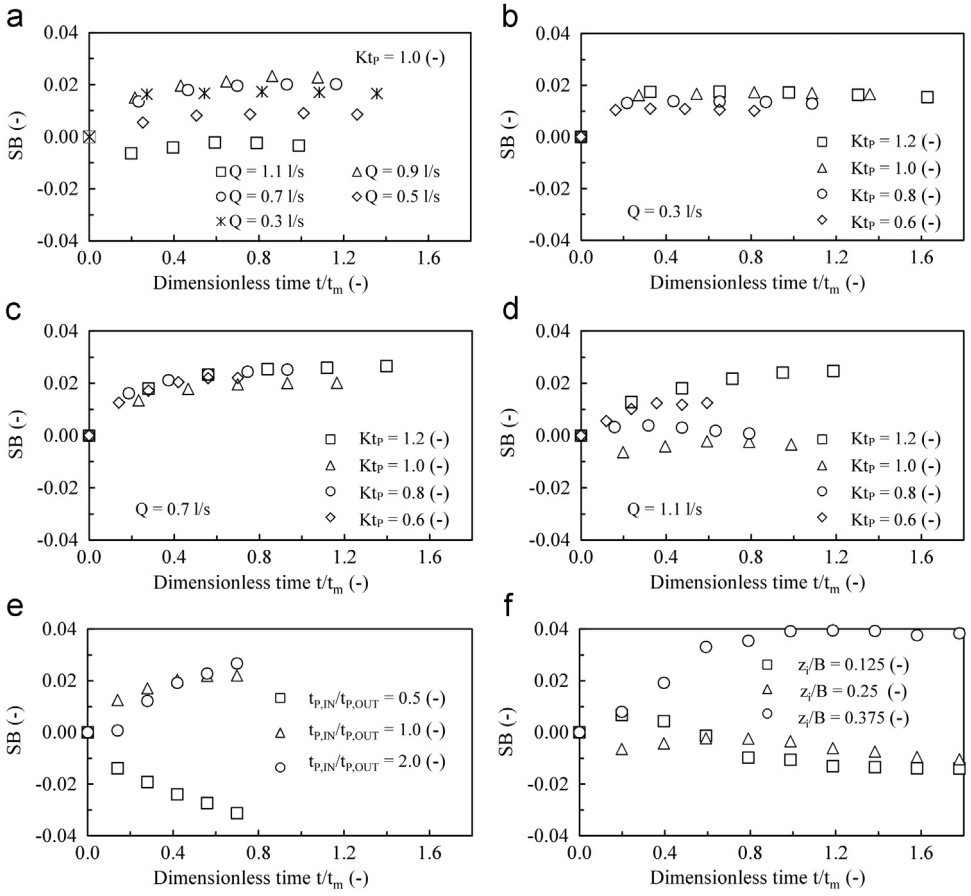

Fig. 11. Sediment balance, *SB*, as a function of dimensionless time, t/t_m, for C_0=0.8 g/l, Kt_P =1.0, and different discharges, *Q* (a), for different cycle frequencies, Kt_P, and discharges *Q*=0.3 (b), 0.7 (c), and 1.1 l/s (d), for *Q*=0.7 l/s and different relative sequence durations, $t_{P,IN}/t_{P,OUT.}$ (e), and for *Q*=1.1 l/s and different intake positions, z_i/B_{MB} (f).

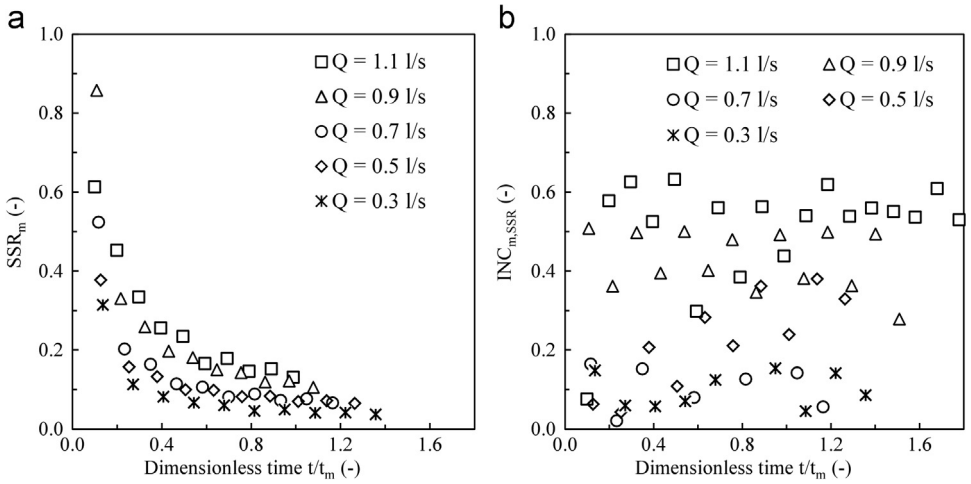

Fig. 12. Mean suspended sediment ratio, SSR_m, (a) and mean relative increase, $INC_{m,SSR}$, (b) as a function of dimensionless time, t/t_m, for five different discharges.

from the inflow and outflow cycles' magnitude or frequency. Therefore, the evolution of suspended sediment ratios, $SSR < 0.4$, (Fig. 12a) is of major interest for the induced cycle analysis.

5.1. Cycle magnitude

Fig. 12 shows the mean suspended sediment ratios SSR_m, as well as the mean relative increase, $INC_{m,SSR}$, as a function of t/t_m. For low discharges, *Q*=0.3 to 0.7 l/s, corresponding to $t_m \geq$ 12,881 s, *SSR* can be increased by 10 to 40% compared to a scenario without operation. Evolution of *SSR* is not well correlated to the inflow and outflow cycles. For higher cycle magnitudes, *Q*=0.9 and 1.1 l/s, corresponding to $t_m \leq$ 8197 s, evolution of SSR correlates with discharge cycles and the suspended sediment ratio increases by 50–60% (Fig. 12b). The remaining $SSR_{m,final}$ at the end of five cycles are listed in Table 2 and shown in Fig. 13.

Increased inflow and outflow cycle magnitude leads to higher overall *SSR* and correlations with the discharge cycles. Thus, *SSR* is

Table 2
Discharge, Q, corresponding mean residence time, t_m, and suspended sediment ratio, $SSR_{m,final}$, for different cycle frequencies, Kt_P.

Q [l/s]	t_m [s]	Kt_P [-]	$SSR_{m,final}$ [%]
0.3	30,056	0.6	5.5
		0.8	5.6
		1.0	3.7
		1.2	3.8
0.5	18,034	1.0	6.5
0.7	12,881	0.6	8.7
		0.8	7.8
		1.0	6.7
		1.2	6.7
0.9	10,019	1.0	10.6
1.1	8,197	0.6	18.2
		0.8	17.9
		1.0	13.2
		1.2	11.0

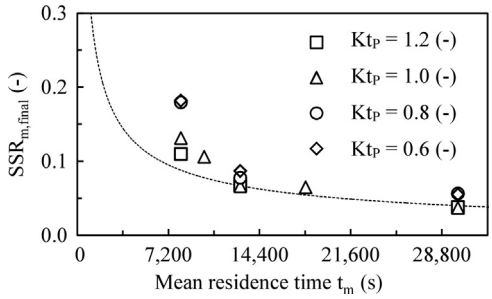

Fig. 13. Mean suspended sediment ratio at the end of the experiment, $SSR_{m,final}$, as a function of mean residence time, t_m, for different cycle frequencies, Kt_P.

higher during inflow sequences and lower during outflow sequences.The systematically increasing *SSR* during inflow sequences could have three origins.

1. First, suspended sediment from the mixing tank enters the main basin. However, quantities from the mixing tank are not high enough to explain the difference of 10 to 20% between inflow and outflow sequences.
2. Second, resuspension of already settled particles could occur. This contribution to the increase of *SSR* could not be quantified in the experiments, but is expected to be very small due to very low flow velocities near the bottom.
3. Third, the main reason for the higher *SSR* during inflow sequences, the kinetic energy input from the entering jet allows mixing of the chamber. Hence, particles that have settled are again moved vertically as well as horizontally in the water body due to the induced flow patterns, and *SSR* increases.

Continuous inflow and outflow sequences for the two highest discharges allow an increase of the mid-term suspended sediment ratio by 50 to 60%.

5.2. Cycle frequency

Results of the parametric study on cycle frequency are shown in Fig. 14. Increased cycle frequencies, Kt_P=0.6 or 0.8, inhibit the evolution of steady flow conditions in the main basin. The evolution of *SSR* is highly fluctuating and does not correlate with the discharge cycles.

In case of low discharges, Q = 0.3 and 0.7 l/s, this is for $t_m \geq 12{,}881$ s, no clear tendency is observed for the different configurations. *SSR* is increased by 5–40% after the five inflow and outflow cycles (Fig. 14a, b). Short sequences never provide sufficient time to reach steady state conditions, influencing mixing efficiency.

For t_m=8197 s (Q =1.1 l/s) the temporal evolution of *SSR*is correlated with the discharge cycles, for all tested frequencies (Fig. 14c). High cycle frequency leads to mean suspended sediment ratios, SSR_m, by 60–80% higher than without operation, for Kt_P=1.0 and 1.2 this reduces to 60% and 50%, respectively (Table 2). Generally, increasing cycle frequency combined with high cycle magnitude leads to higher *SSR* in the system, due to high kinetic energy input during inflow sequences and fast changes in flow direction. Especially during the first settling period, cycle frequency is a key parameter affecting the efficiency of the entire operational sequence. If in this phase high cycle frequency is applied, the *SSR* can be considerably increased for the first cycles as well as for durations up to t/t_m=1.2.

5.3. Relative sequence duration

The inflow and outflow cycles observed in engineering applications are rarely regular in magnitude and frequency. Thus, in addition to the tested ranges of discharges and cycle duration, the relative sequence duration, $t_{P,IN}/t_{P,OUT}$, was varied in two tests. For an inflow sequence of half of the outflow sequence, a net water withdrawal from the main basin results. The opposite scenario consists in a reduction in outflow to half of the inflow sequence duration.

Fig. 15 shows that a relative sequence duration $t_{P,IN}/t_{P,OUT}$=2.0 results in considerably higher suspended sediment ratios. Inflow sequences are intercepted by shorter outflow sequences. Particle settling is reduced due to frequent and repetitive increase of turbulence in the test chamber. The mean relative increase achieves 50% and at the end of five cycles $INC_{m,SSR}$=0.43.

5.4. Initial sediment concentration

The initial sediment concentration influences the suspended sediment ratio, *SSR*, by up to 40%. Compared to the reference state without operation, higher initial sediment concentration leads to increased *SSR*, as shown in Fig. 16. While for C_0 = 0.3 and 0.8 g/l the mean relative error fluctuates around $INC_{m,SSR}$ = 0.10 where as $INC_{m,SSR}$ = 0.30 for C_0 = 1.5 g/l.

5.5. Intake position

Fig. 17 shows the results for three prolongated tests for t_m=8197 s, Kt_P=1.0, and different intake positions, z_i/B_{MB}, above the reservoir bottom. On the one hand, inflow and outflow sequences increase *SSR* not only over five cycles, but also over up to ten inflow and outflow cycles. On the other hand, an intake located closer to the reservoir bottom or to the free surface generates flow conditions to keep fine sediment in suspension. For an intake position closer to the bottom (z_i/B_{MB}=0.125) or the free water surface (z_i/B_{MB}=0.375), *SSR* ratios are up to 80% higher than for the reference test and 20% higher compared to the initial intake position, z_i/B_{MB}=0.25. Amplified vertical recirculation keeps more particles in suspension.

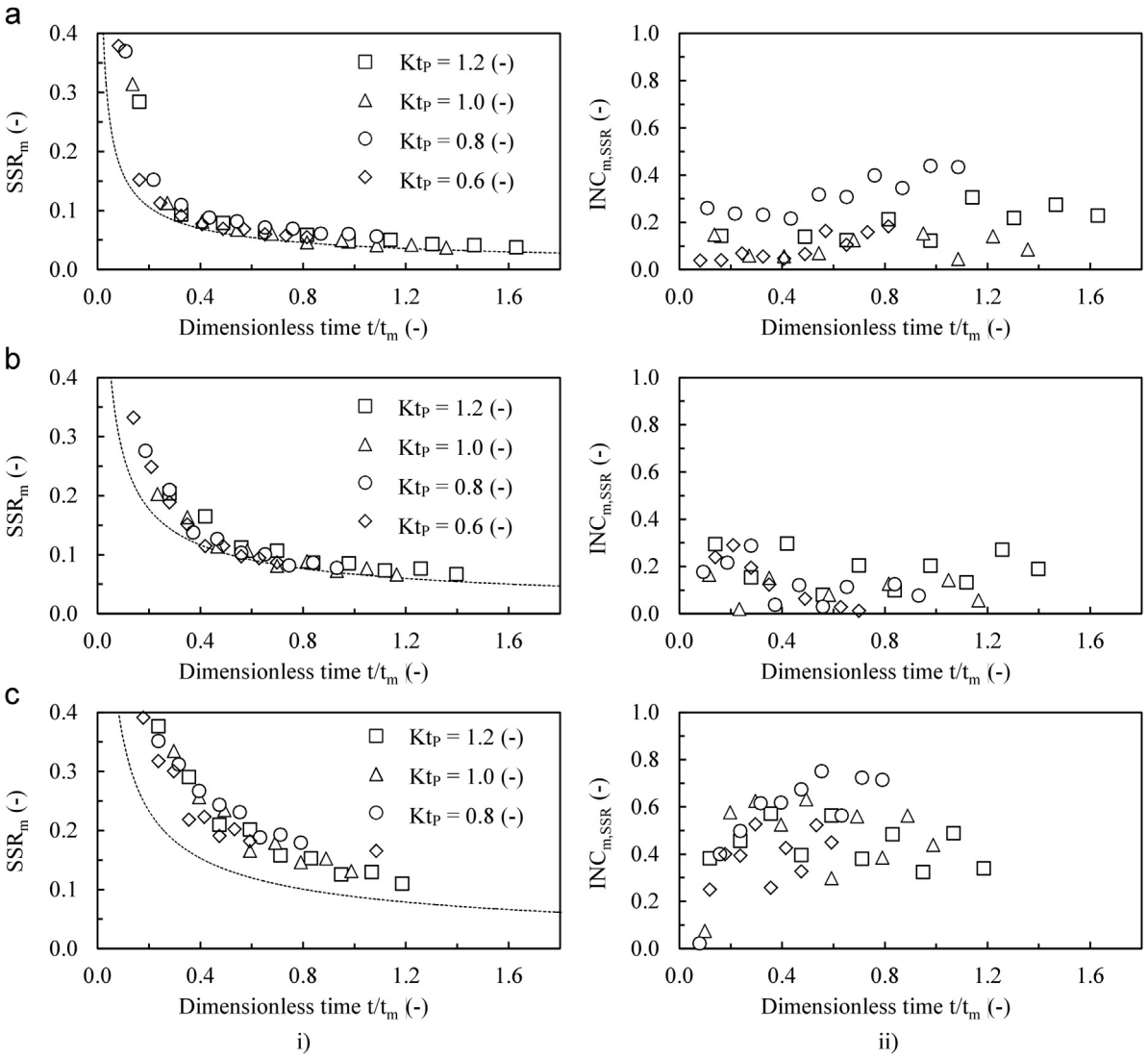

Fig. 14. Mean suspended sediment ratio, SSR_m, (i) and mean relative increase, $INC_{m,SSR}$, (ii) as a function of dimensionless time, t/t_m, for C_0=0.8 g/l, with different cycle frequencies, Kt_P, and discharges Q=0.3 (a), 0.7 (b), and 1.1 l/s (c). The dashed line represents the settling curve of suspended sediment in stagnant water.

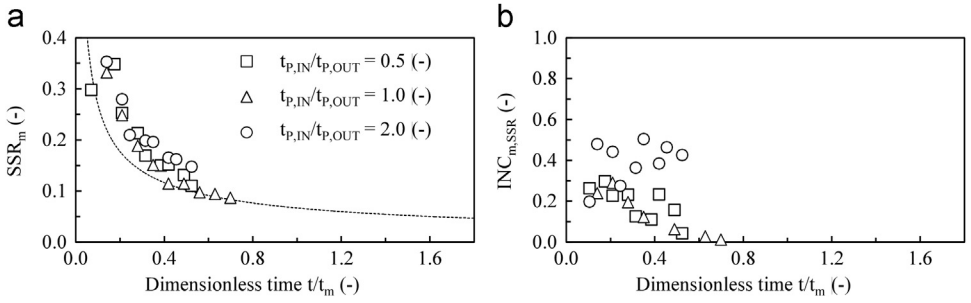

Fig. 15. Mean suspended sediment ratio, SSR_m, (a) and mean relative increase, $INC_{m,SSR}$, (b) as a function of dimensionless time, t/t_m, for C_0 = 0.8 g/l, Kt_P = 0.6, Q = 0.7 l/s, and different relative sequence durations, $t_{P,IN}/t_{P,OUT}$. The dashed line represents the settling curve of suspended sediment in stagnant water.

6. Conclusions

The influence of repetitive inflow and outflow sequences on the suspended sediment settling processes of a system consisting of two connected reservoirs was studied in laboratory experiments. Test results reveal that settling of fine particles near an intake/outlet structure can be considerably reduced by inflow and outflow sequences. Compared to “no operation” conditions with settling of fine sediment in stagnant water, the amount of fine particles kept in suspension by inflow and outflow discharge is increased by up to 80%, depending on cycle magnitude and frequency as well as the intake location above the reservoir bottom. High cycle magnitude and frequency lead to the maximum suspended sediment ratio in the system, correlated to the inflow and outflow cycles.For all tested configurations, the sediment balance of the system remains in equilibrium, indicating that the influx

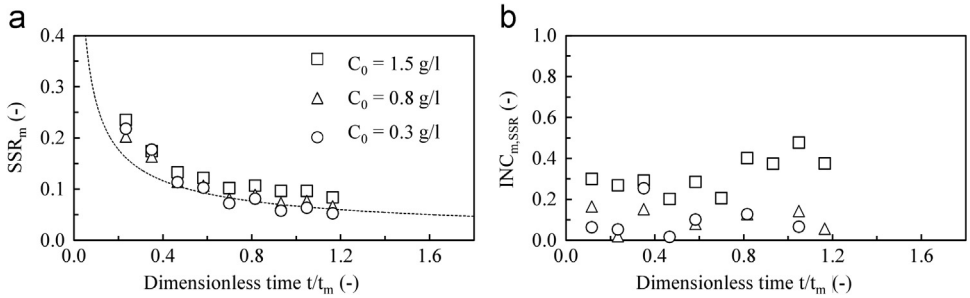

Fig. 16. Mean suspended sediment ratio, SSR_m, (a) and mean relative increase, $INC_{m,SSR}$, (b) as a function of dimensionless time, t/t_m, for $Kt_P = 0.6$, $Q = 0.7$ l/s, and different initial sediment concentrations, C_0. The dashed line represents the settling curve of suspended sediment in stagnant water.

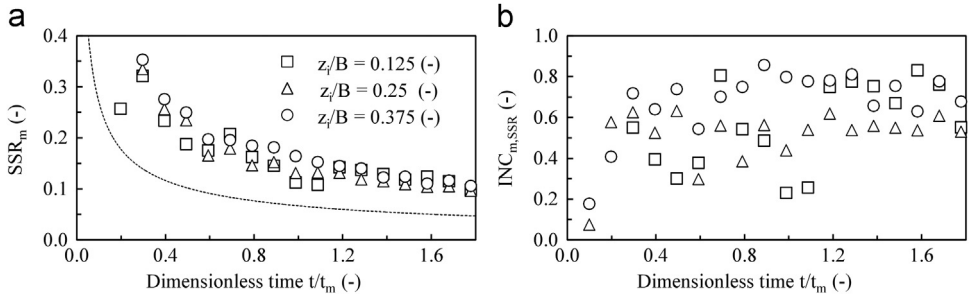

Fig. 17. Mean suspended sediment ratio, SSR_m, (a) and mean relative increase, $INC_{m,SSR}$, (b) as a function of dimensionless time, t/t_m, for $C_0 = 0.8$ g/l, $Kt_P = 1.0$, $Q = 1.1$ l/s, and different intake positions, z_i/B_{MB}. The dashed line represents the settling curve of suspended sediment in stagnant water.

and evacuated sediment rates are not significantly influenced by the inflow and outflow cycles.

Applied to a real-life problem, i.e. the arrival and deposition of a turbidity current in the area of a pumped-storage intake/outlet structure, it is expected that important settling occurs during the first hours after the turbidity current event, which cannot entirely be avoided by an adequate plant operation. However, according to experimental results, the quantity of fine sediment kept in suspension can be considerably increased when operating the plant at high discharge and with short pumped-storage sequences in this phase. Later on, pumped-storage operation at a high cycle magnitude is the most promising measure to slow down sediment settling.

Acknowledgements

The presented laboratory work was conducted in the framework of the *HydroNet*project consortium funded by the *Competence Center Energy and Mobility* (CCEM), *Swisselectric Research* and the *Swiss Federal Office of Energy* (SFOE – *Hydropower Research*). Thanks are expressed to L. Bremen and A. Pachoud for their conscientous work related to preliminary experiments and preliminary numerical modeling.

References

Anderson, M. A. (2010). Influence of pumped-storage hydroelectric plant operation on a shallow polymictic lake: Predictions from 3-D hydrodynamic modeling. *Lake and Reservoir Management*, *26*(1), 1–13.

Basson, G.R. (2009). Management of siltation in existing and new reservoirs. General Report Q89. In *Proceedings (on CD) of the 23rd congress of the International Commission on Large Dams CIGB-ICOLD*, May 25–29, 2009, Brasilia, Vol. II.

Batuca, D.G., & Jordaan, J.M. (2000). *Silting and Desilting of Reservoirs*. A.A. Balkema, Rotterdam.

Boillat, J. L., & Delley, P. (1992). Transformation de la prise d'eau de Malvaglia, étude sur modèle et réalisation. *Wasser, Energie, Luft - Eau, Energie, Air*, *84*(7), 145–151. (*In French*)

Boillat, J.L., & Pougatsch, H. (2000). State of the art of sediment management in Switzerland. In *Proceedings of international workshop and symposium on reservoir sedimentation management* (pp 35-45). Tokyo, Japan.

Bonalumi, M., Anselmetti, F. S., Kaegi, R., & Wüest, A. (2011). Particle dynamics in high-Alpine proglacial reservoirs modified by pumped-storage operation. *Water Resources Research*, *47*(9), W09523. http://dx.doi.org/10.1029/2010WR010262.

Cardoso, S. S. S., & Zarrebini, M. (2001a). Convection driven by particle settling surrounding a turbulent plume. *Chemical Engineering Science*, *56*(11), 3365–3375.

Cardoso, S. S. S., & Zarrebini, M. (2001b). Sedimentation of polydispersed particles from a turbulent plume. *Chemical Engineering Science*, *56*(16), 4725–4736.

Cuthbertson, A. J. S., & Davies, P. A. (2008). Deposition from particle-laden, round, turbulent, horizontal, buoyant jets in stationary and coflowing receiving fluids. *Journal of Hydraulic Engineering*, *134*(4), 390–402.

De Cesare, G., & Schleiss, A.J. (1999). Turbidity current monitoring in a physical model flume using ultrasonic Doppler method. In *Proceedings of the 2nd international symposium on ultrasonic Doppler methods for fluid mechanics and fluid engineering* (pp. 61–64). Villigen, Switzerland.

De Cesare, G., Schleiss, A. J., & Hermann, F. (2001). Impact of turbidity currents on reservoir sedimentation. *Journal of Hydraulic Engineering*, *127*(1), 6–16.

Ernst, G. G. J., Sparks, R. S. J., Carey, S. N., & Bursik, M. I. (1996). Sedimentation from turbulent jets and plumes. *Journal of Geophysical Research*, *101*(B3), 5575–5589.

Imboden, D. (1980). The impact of pumped storage operation on the vertical temperature structure in a deep lake: a mathematical model. In *Proceedings of the Clemson workshop on environmental impacts of pumped storage hydroelectric operations* (pp. 125–146). Clemson, South Carolina, US.

Jenzer Althaus, J. (2011). *Sediment evacuation from reservoirs through intakes by jet induced flow* (Doctoral dissertation) In: A. Schleiss (Ed.), *Communication No 45 du Laboratoire de constructions hydrauliques*. Lausanne, Switzerland: Ecole Polytechnique Fédérale de Lausanne (Thesis 4927).

Kantoush, S. A., De Cesare, G., Boillat, J. L., & Schleiss, A. J. (2008). Flow field investigation in a rectangular shallow reservoir using UVP, LSPIV and numerical modelling. *Flow Measurement and Instrumentation*, *19*(3–4), 139–144.

Knoblauch, H., Hartmann, S., & De Cesare, G. (2005). Sedimentmanagement an alpinen Speichern: Das EU-INTERREG IIIB Projekt ALPRESERV. *Österreichische Wasser- und Abfallwirtschaft*, *57*(11), 185–190. (*In German*)

Lane-Serff, G. F., & Moran, T. J. (2005). Sedimentation from buoyant jets. *Journal of Hydraulic Engineering*, *131*(3), 166–174.

Met-Flow SA (2000). *UVP monitor - User's guide*. Lausanne, Switzerland.

Müller, M. (2012). *Influence of in- and outflow sequences on flow patterns and suspended sediment behavior in reservoirs* (Doctoral dissertation) In: A. Schleiss (Ed.), *Communication N° 53 du Laboratoire de constructions hydrauliques*. Lausanne, Switzerland: Ecole Polytechnique Fédérale de Lausanne (Thesis 5471).

Müller, M., De Cesare, G., & Schleiss, A. J. (2014). Continuous long-term observation of suspended sediment transport between two pumped-storage reservoirs. *Journal of Hydraulic Engineering*, *140*(5), 637–648.

Oehy, C. D., De Cesare, G., & Schleiss, A. J. (2010). Effect of inclined jet screen on turbidity current. *Journal of Hydraulic Research*, *48*(1), 81–90.

Oehy, C. D., & Schleiss, A. J. (2007). Control of turbidity currents in reservoirs by solid and permeable obstacles. *Journal of Hydraulic Engineering*, *133*(6), 637–648.
Qi, M., Fujisak, K., & Tanaka, K. (2000). Sediment re-suspension by turbulent jet in an intake pond. *Journal of Hydraulic Research*, *38*(5), 323–330.
Schleiss, A. J., De Cesare, G., & Jenzer Althaus, J. (2010). Verlandung der Stauseen gefährdet die nachhaltige Nutzung der Wasserkraft. *Wasser, Energie, Luft – Eau, Energie, Air*, *102*(1), 31–40. (*In German*)
Schleiss, A. J., Franca, M. J., Juez, C., & De Cesare, G. (2016). Reservoir sedimentation. *Journal of Hydraulic Research*, *54*(6), 595–614 (Vision paper).
Stefan, H. G., & Gu, R. (1992). Efficiency of jet mixing of temperature-stratified water. *Journal of Environmental Engineering*, *118*(3), 363–379.
Takeda, Y. (1995). Velocity profile measurement by ultrasonic doppler method. *Experimental Thermal and Fluid Science*, *10*(4), 444–453.
Toniolo, H., & Schultz, J. (2005). Experiments on sediment trap efficiency in reservoirs. *Lakes & Reservoirs: Research & Management*, *10*(1), 13–24.
U.S.Bureau of Reclamation (1993). *Aquatic ecology studies of Twin Lakes, Colorado, 1971-86: Effects of a pumped-storage hydroelectric project on a pair of montane lakes* (Monograph No. 43). Denver, Colorado.
van Rijn, L. C. (1984). Sediment transport, Part II: Suspended load transport. *Journal of Hydraulic Engineering*, *110*(11), 1613–1641.
Wasewar, K. L. (2006). A design of jet mixed tank. *Chemical and Biochemical Engineering Quarterly*, *20*(1), 31–45.
Yu, W. S., Lee, H. Y., & Hsu, S. M. (2000). Experiments on deposition behavior of fine sediment in a reservoir. *Journal of Hydraulic Engineering*, *126*(12), 912–920.